Electrochemical Changes in Lithium-Battery Electrodes Studied Using 7Li NMR and Enhanced 13C NMR of Graphene and Graphitic Carbons

Kristopher J. Harris,[†] Zoë E. M. Reeve,[†] Dongniu Wang,[‡] Xifei Li,[‡] Xueliang Sun,[‡] and Gillian R. Goward*,[†]

[†]Department of Chemistry, McMaster University, Hamilton, Ontario L8S 4M1 Canada
[‡]Department of Mechanical and Materials Engineering, University of Western Ontario, London, Ontario N6A 5B9 Canada

S *Supporting Information*

ABSTRACT: An anode composed of tin-core, graphitic-carbon-shell nanoparticles distributed on graphene nanosheets, Sn@C-GNs, is studied during the lithiation process. 7Li NMR provides an accurate measure of the stepwise reduction of metallic Sn to lithium−tin alloys and reduction of the graphitic carbon. The metallic nanoparticle cores are observed to form ordered, crystalline phases at each step of the lithiation process. The 7Li 2D experiments presented provide insight into the proximity of the various phases, reflecting the mechanism of the electrochemical reaction. In particular, a sequential model of nanoparticle lithiation, rather than a simultaneous process, is suggested. Movement of lithium ions between two elements of the nanostructured Sn@C-GNs material,

the metallic core and carbon shell, is also observed. Conventional 13C solid-state NMR, SSNMR, experiments on <5 mg of active material from electrochemical cells were found to be impossible, but signal enhancements (up to 18-fold) via the use of extended echo trains in conjunction with magic-angle spinning enabled NMR characterization of the carbon. We demonstrate that the 13C data is extremely sensitive to the added electron density when the graphitic carbon is reduced. We also investigate ex situ carbon electrodes from cycled Li−O2 cells, where we find no evidence of charge sharing between the electrochemically active species and the graphitic carbon in the 13C NMR spectroscopy.
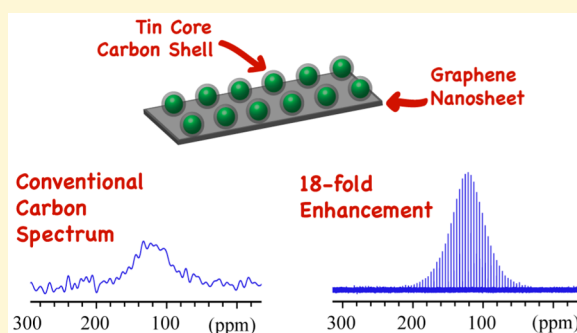
■ INTRODUCTION

Lithium ion batteries play an ever increasing role in the energy economy, but current industrialized cell technologies still suffer from unfortunate limitations. Higher energy capacities and reductions in capacity losses due to undesirable side reactions currently form an intensive area of research. Rational design of next generation lithium-battery materials requires a detailed understanding of not only the structures but also the changes induced by electrochemical cycling.

A hierarchically nanostructured anode, shown schematically in Figure 1a and by TEM microscopy in Figure 1b, is studied during electrochemical cycling. The material is composed of 50−100 nm Sn nanoparticles, each coated with an approximately 50 nm thick carbon shell, distributed in a uniform, dense layer on graphene nanosheets (Sn@C-GNs). While most tin-based anodes fail prematurely due to mechanical fracturing and electrical isolation of large portions of the material,[1,2] Sn@C-GNs have recently been shown to combine some of the high capacity of metallic tin with the excellent stability of carbon.[3] Despite the excellent anodic perfomance, important questions regarding specific details of the structure and its evolution during the charge cycle remain. Of particular interest are details of the structure of the carbon shell as well as the stepwise

reduction of the metallic tin core and the carbon shell. Here, we employ solid-state NMR, SSNMR, spectroscopy to provide high resolution measurements of these phenomena.

We demonstrate that 7Li NMR provides a sensitive report of the anodic reduction. 1D 7Li NMR yields an excellent measure of the state of charge of the Sn@C-GNs anode, by measuring the specific Li−Sn alloys formed and the lithiated carbon shells of the nanoparticles. Furthermore, we develop 2D 7Li exchange NMR experiments as a means of providing insight into the reduction mechanism through measurement of the proximity of each reduced species. The 7Li spectra show clear evidence that the reduction is heterogeneous across the electrode, rather than a homogeneous reduction of all nanoparticles simultaneously.

The graphitic carbon portion of the composite anode is involved in the reduction process and is studied via 13C SSNMR. The 13C spectra are sensitive to the chemical structure of the carbonaceous portion of the anode, and it is furthermore demonstrated that the lifetimes of the 13C nuclear spin states are extremely sensitive to reduction. This sensitivity is used to
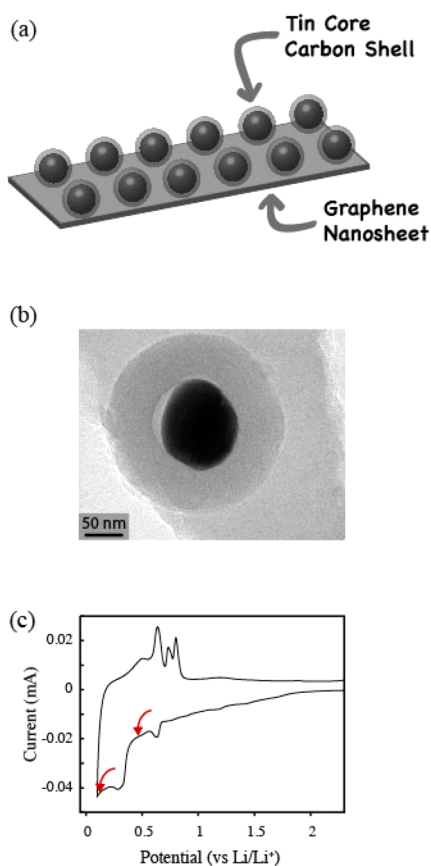
Figure 1. (a, b) Schematic representation and TEM image of the hierarchical Sn@C-GNs nanostructure. (c) Cyclic voltammogram of Sn@C-GNs. Red arrows mark the voltages at which cells were stopped for NMR analysis.

investigate electron sharing between the metallic core and graphitic shell of the nanoparticles.

We note that we were forced to explore signal enhancement techniques to collect useful ^{13}C spectra given the small sample sizes and well-known difficulties associated with ^{13}C NMR spectroscopy of nonprotonated sites with broad line widths. We report that the Carr-Purcell/Meiboom-Gill (CPMG)[4,5] method of signal enhancement, previously unexplored for ^{13}C spectroscopy of magic-angle spinning (MAS) samples, provides access to the otherwise unavailable ^{13}C spectra of the electrochemical samples. The CPMG-MAS method should prove useful in many studies given the well-proven relationship of ^{13}C spectra to structure in materials such as graphene and graphene oxide,[6−8] disordered nanodiamonds,[9] and diamond-like thin carbon films.[10,11] Potential future applications include nonprotonated carbon sites ubiquitous not only in battery technology but also in electronics, photonics, spintronics, fuel cells, solar cells, etc.

As a means of providing better context for the CPMG-MAS data, a graphitic carbon electrode from a different type of lithium ion battery was also investigated: that from an Li−O$_2$ cell. In Li−O$_2$ cells, a graphitic carbon electrode is used to bring about oxidation of O$_2$ to Li$_2$O$_2$ (in ideal cases).[12,13] The graphitic electrode in an Li−O$_2$ cell is involved in the redox process but is not itself a final oxidation or reduction product in the reaction. Because this mode contrasts with the direct reduction of graphitic carbon in Sn@C-GNs, it is interesting to monitor the Li−O$_2$ cell electrode with the developed ^{13}C

CPMG-MAS method. The spectra are used to look for evidence of any structural changes in the electrode and to check for possible reduction electrons stored within the graphitic carbon.

Below, we present a physical characterization of two types of lithium battery electrodes at different points in the charge cycle using SSNMR. 1D and 2D ^{7}Li NMR experiments on electrochemically cycled Sn@C-GNs are presented first. These results are used to provide insight into the species formed and mechanism of the reduction process. Benchmark ^{13}C CPMG-MAS NMR experiments conducted on pristine graphene nanosheets are then used to validate the method and demonstrate its benefits. ^{13}C CPMG-MAS measurements on the electrochemically cycled Sn@C-GNs are then presented. Finally, ^{13}C measurements on the graphitic carbon electrode of an Li−O$_2$ cell, which highlight contrasting redox behavior to the Sn@C-GNs system, are discussed.

■ EXPERIMENTAL SECTION

Graphene nanosheets for Sn@C-GNs were synthesized by heating graphene oxide (from a modified Hummers procedure on graphite) at 1050 °C in an Ar atmosphere. Carbon-coated Sn nanoparticles distributed on graphene nanosheets were synthesized by distributing commercial 325 mesh SnO$_2$ particles on GNs via sonication in ethanol, followed by reduction with 10/90 ethylene−argon gas at 800 °C. See Wang et al.[3] for further details and extensive physical characterization of identically produced Sn@C-GNs.

Electrochemical cells of both Sn@C-GNs and Li−O$_2$ systems were assembled versus metallic Li in CR2032 coin cell bodies, using Celgard separators. Electrode discs of Sn@C-GNs were prepared on copper as a slurry in NMP with 10% conductive carbon black and 10% polyvinylidene fluoride (by weight) and used in electrochemical cells with 1 M LiPF$_6$ in 50/50 ethylene carbonate/dimethyl carbonate (by volume) as electrolyte. Sn@C-GNs cells were discharged at rates between 8 and 19 mA/g. Cathode electrodes for Li−O$_2$ cells were prepared as free-standing, porous composites from slurries prepared by mixing Super C65 carbon black (Timcal), polyvinylidene fluoride, and dibutyl phthalate in a weight ratio of 0.625:1:1. The dibutyl phthalate was removed by washing with dry diethyl ether followed by drying for 2 h at 70 °C. The Li−O$_2$ cathodes were cycled at a rate of 70 mA/g until the desired capacity was reached.

Electrochemical cycling was performed on Li−O$_2$ cells in a glass chamber under O$_2$ gas, which accesses the porous electrode through perforations in the battery casing, using a 1 M solution of lithium bis(trifluoromethanesulfonyl)imide in trimethylphosphate as the electrolyte. The electrochemical cells were disassembled in an Ar atmosphere; the relevant electrodes were washed with dry/deoxygenated propylene carbonate (Sn@C-GNs cells) or acetonitrile (Li−O$_2$ cells) and dried under vacuum, and the powders mechanically separated from the support.

All NMR experiments were carried out at 11.75 T with a Bruker Avance I spectrometer using 2.5 mm diameter rotors, which were center packed using a spacer of dry alumina powder when available sample sizes were less than the rotor volume. ^{1}H MAS NMR spectroscopy, which has a very high sensitivity per unit mass, was applied to the Sn@C-GNs. The lack of observable ^{1}H signal demonstrates that the ethylene gas reactant is essentially completely reduced. The ^{7}Li spectra were recorded at 20 kHz (0.4 V sample) and 29 kHz (0.01 V sample) sample spinning, using a rotor synchronized echo pulse sequence with 62.5 kHz rf power and a 10 s recycle delay; chemical shifts were referenced to 1 M LiCl(aq) at 0 ppm. ^{13}C spectra were recorded under 20 kHz MAS using 62.5 kHz rf power levels and 40 rotor-period acquisition windows, without the use of proton decoupling pulses. Carbon chemical shifts were referenced to the high-frequency peak of an external sample of adamantane at 38.5 ppm, while recycle delays were optimized on pristine samples, with 60 s being employed in all cases.

■ RESULTS AND DISCUSSION

Sn@C-GNs provide intriguing electrochemical performance by combining some of the favorable characteristics of the metallic tin and graphitic carbon components. A CV of the material, Figure 1c, shows distinct reduction peaks at 0.65 and 0.35 V from the alloying of metallic tin cores and shows further reduction near 0 V from lithiation of the graphitic carbon.[3] The nonzero slope of the reduction half of the CV away from the reduction peaks is likely due to a combination of SEI formation and some heterogeneity in the reduction potentials in the complex material, particularly in the disordered carbon layer. For a more complete discussion of the CV of the material, including multiscan CV, see ref 3. Sn@C-GNs show a discharge capacity of 566 mAh/g after 100 cycles, midway between the 372 and 994 mAh/g theoretical capacities for graphite and metallic tin, respectively. The midway capacity is sensible given that the hybrid material is 78% Sn by weight, and the carbon shells may have a somewhat limiting effect on the volume expansion required by alloy formation.

Coin cells comprised of Sn@C-GNs anodes were discharged under a constant current until reaching a voltage of either 0.4 or 0.01 V, i.e., just before the second reduction peak of the tin cores seen in the CV and near complete reduction (with measured discharge capacities of 290 and 560 mAh/g). The cells were then disassembled and the electrode powders mechanically separated from the support and packed into NMR rotors.

^{7}Li NMR of Sn@C-GNs. The ^{7}Li NMR spectra, Figure 2, of the charged active materials are assigned using published
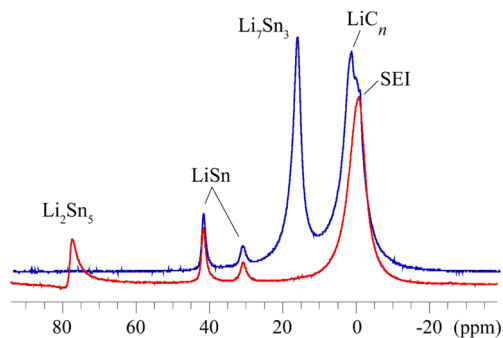

Figure 2. Lithium-7 ex situ MAS NMR spectra of powdered Sn@C-GNs electrodes after electrochemical discharge. The isotropic peak regions of spectra collected using Hahn echoes with total echo-delay times of 96 and 68 μs collected from Sn@C-GNs at 0.4 V vs Li/Li$^+$ (red) and 0.01 V (blue) are shown. The Li$_2$Sn$_5$ peak appears slightly out of phase; likely, this is due to a shallow skin depth of rf penetration in this highly conductive sample creating a range of echo conditions.

data[14−17] to two specific Sn−Li alloy phases for the 0.4 V sample and two Sn−Li alloy phases as well as lithiated carbon for the 0.01 V sample. The spectrum of the 0.4 V sample contains an Li$_2$Sn$_5$ alloy peak at 78.0(5) ppm, a pair of peaks at 42.3(5) and 31.5(5) ppm from the two crystallographic sites in LiSn, and a peak at 0.0(5) ppm that is assigned[16−19] to Li in the solid electrolyte interface (SEI) layer. We note that the SEI peak can be selectively removed from the spectrum with reasonable efficiency using a T$_2$ filter (see the Supporting Information). The spectrum of the 0.01 V sample again shows the pair of LiSn alloy peaks as well as a peak at 17.0(5) ppm that we assign to the Li$_7$Sn$_3$ given its reported chemical shift of 17.3 ppm. The remaining peak at 2.0(5) ppm is inconsistent

with the chemical shift and line width of any known lithium−tin alloy[14] or SEI phases.[20] It is, however, a close match with observations of partially lithiated graphitic carbons[16,18] and is assigned as such.

Clearly, the ^{7}Li MAS NMR spectra provide a useful monitor of the electrochemical reaction taking place in the hybrid anode. The peaks appear at the same chemical shift as the crystalline reference materials,[14] are narrow, and do not show evidence of shifting with the charge state. This behavior reflects the formation of specific, crystalline phases in the nanoparticle cores, rather than reduction via a disordered, glassy insertion model. The observation of multiple phases with distinct redox potentials may be related to small differences in electric potential across the complicated electrode. The reduction process appears to involve reduction of the metallic core via a progression through the large phase table of crystalline Sn−Li alloys, with ever increasing Li content; once the potential is lowered sufficiently, lithiation of the carbonaceous shell commences as it becomes competitive.

In situ X-ray diffraction, electron diffraction, and atomic force microscopy have also been employed to track the sequence of lithiation products generated during discharge of Sn-based anodes.[21−25] All of the diffraction studies have clearly shown the presence of Li$_2$Sn$_5$ as the first step in the lithiation process.[22−25] X-ray diffraction studies showed LiSn as the subsequent step in the progression, appearing near 0.4 V vs Li/Li$^+$,[22,23,25] and localized electron diffraction showed lattice spacing consistent with LiSn (though definitive assignment as LiSn was not possible).[24] However, the next phase in the lithiation process was not observable via diffraction methods, perhaps due to small particle size or amorphous character.[25] The presence of this intermediate phase was only observable indirectly, as a loss of total diffraction intensity and a physical increase of the particle sizes during this step of lithiation.[21,25] In contrast, the NMR results provide a definitive measurement of Li$_7$Sn$_3$ as the lithiation product following LiSn.

Transfer of Li$^+$ between the different components of the charged electrode might be expected if they are close to each other, and such motion was investigated using 2D ^{7}Li exchange spectroscopy, EXSY. In the EXSY experiment, the chemical shift is measured before and after a mixing period, τ_{mix}, such that any Li atoms which move between NMR-resolved locations during τ_{mix} appear at different frequencies in the two dimensions, i.e., are seen as peaks off the main diagonal. The 0.4 V sample of Sn@C-GNs contains ^{7}Li NMR sites from lithium in three components: Li$_2$Sn$_5$ alloy at 78.0 ppm, LiSn alloy at 42.3 and 31.5 ppm, and SEI at 0 ppm. The EXSY spectrum of the 0.4 V sample of Sn@C-GNs, Figure 3a, reflects exchange between the two crystallographic sites in the LiSn alloy at τ_{mix} = 0.5 s. Evidence of this exchange is observed with τ_{mix} as short as 100 ms, as expected for this excellent Li conductor.[14] Mixing times up to 1 s were investigated, but no lithium motion between the two distinct alloy phases or involving the SEI layer is observed. Obviously, very long mixing times would eventually show Li exchange between all sites in ionically conductive anodes (provided spin-state lifetimes are sufficient), but the interest here is in using short mixing times to probe proximate sites.

Dynamics in the 0.01 V sample of Sn@C-GNs were also investigated using EXSY. This sample is characterized by ^{7}Li NMR sites chiefly from 4 phases: LiSn alloy at 42.3 and 31.5 ppm, Li$_7$Sn$_3$ at 17.3 ppm, Li in the carbon shell at 2.0 ppm, and SEI at 0 ppm. The EXSY spectrum of the 0.01 V sample of
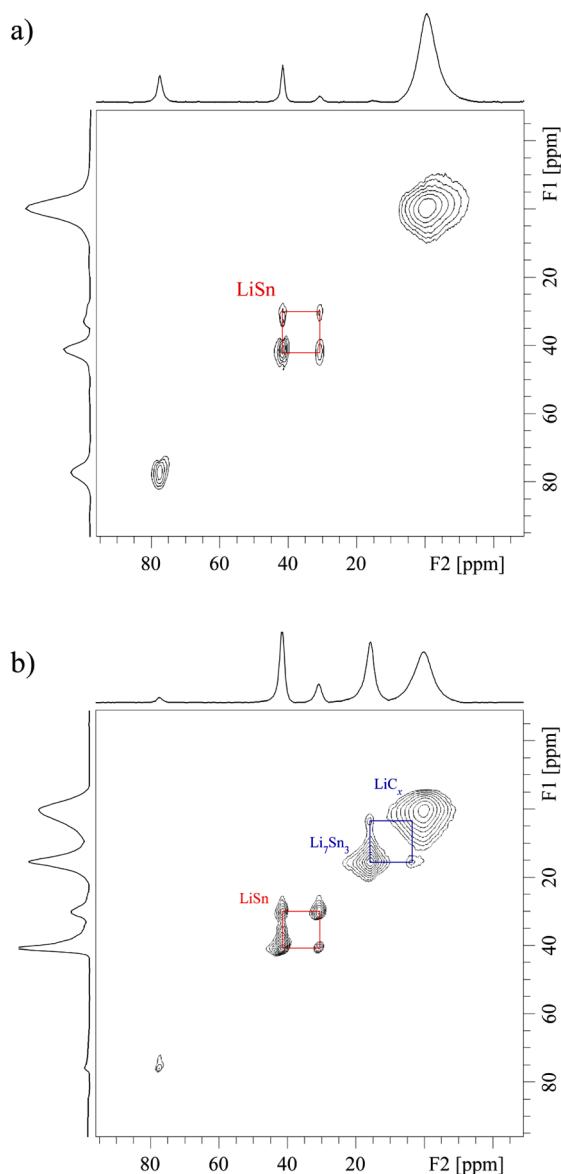
a)

b)

Figure 3. Lithium-7 EXSY NMR spectra of powdered Sn@C-GNs electrodes after electrochemical discharge. (a) Spectrum of Sn@C-GNs discharged to 0.4 V vs Li/Li⁺, collected with a 0.5 s mixing time over a period of 17 h. (b) Spectrum of Sn@C-GNs discharged to 0.01 V vs Li/Li⁺, collected with a 1 s mixing time over a period of 10.5 h. The blue box highlights the location of the off-diagonal peaks, whose frequencies show a correlation of the 2.0 ppm LiC_x peak with the 17 ppm Li_7Sn_3 peak.

Sn@C-GNs collected with τ_{mix} = 1 s, Figure 3b, also evidences the expected exchange between the two sites of LiSn. Again, there is no exchange observed between the three lithium−tin alloys present (there is a small amount of Li_2Sn_5 in this 0.01 V sample) or with the SEI. Contrastingly, chemical exchange is observed between the highest-lithium-content alloy, Li_7Sn_3, and lithium in the carbonaceous shell. It is particularly interesting to see a direct measurement of lithium ions moving between the two components of the heterogeneous nanostructure. The observation of Li exchange between the peaks assigned to Li_7Sn_3 and Li in the carbon shell provides an interesting confirmation of this LiC_x assignment, as it rules out assignment of the 2.0 ppm peak as a second SEI site, given SEI layers occur

at the interface between the electrolyte and the carbon shell, which is distant from the Sn core.

The ⁷Li EXSY spectroscopy provides a more detailed picture of the reduction process in the Sn@C-GNs anode. Lithium ions are highly mobile in all of the lithiated phases present, and exchange with any adjacent phases would be expected, e.g., as seen in the exchange between Li_7Sn_3 and the carbonaceous shell of Figure 3b. The lack of any observable exchange at long mixing times between the distinct Sn−Li phases seen in each sample therefore demonstrates that the nanoparticles in the entire sample are not lithiated simultaneously, as a partially reduced sample generated by such a mechanism would contain an ensemble of nanoparticles with, for example, half Li_2Sn_5 and half LiSn alloys. Such an ensemble of particles composed of half of one phase each would provide ample opportunity for exchange and observable exchange peaks between the phases. Therefore, the mechanism must be much closer to a sequential lithiation, with most nanoparticle cores almost entirely composed of one specific alloy phase. Furthermore, the EXSY data shows that the carbon shell is significantly lithiated only for nanoparticles whose cores are reduced to an Li content equal to at least the Li_7Sn_3 composition, demonstrating the point at which the lithiated carbonaceous shell becomes stable toward oxidation by the metallic nanoparticle core.

EXSY NMR observation of the lithiation process provides interesting complementary data to the picture generated by in situ X-ray[22,23] and electron[24] microscopy/diffraction studies of lithiation in tin anodes. These localized diffraction studies show clear evidence of heterogeneous particles during charging, while the NMR study shows homogeneous particles. In situ X-ray studies of 1 to 15 μm Sn microparticles showed heterogeneous, mixed-phase particles were generated when cycling at a rate of 200 mA/g.[22,23] A lithiated shell 1 to 2 μm thick was observed after partial discharge, and the heterogeneity has been assigned to slow kinetics of the phase transformation required for lithiation.[22,23] Similarly, an in situ electron-microscopy study of 56 nm thick carbon-coated tin nanowires shows that, during a rapid (20 s) discharge, the nanowire was heterogeneously lithiated from one end, with several phases present inside one nanowire.[24] This heterogeneity contrasts with the homogeneous lithiation observed in the present EXSY NMR study of the Sn@C-GNs. Likely, the different behavior can be ascribed to two factors: (i) morphology and (ii) charge rate. (i) Homogeneous lithiation is much more attainable in the 50−100 nm Sn@C nanoparticles than in the 1−15 μm Sn microparticles, despite the use of relatively slow discharge (though the rate employed for the microparticle study was also ca. 10−20 times faster than that used for the Sn@C-GNs). Notably, the regions over which uniform phases were observed in the Sn microparticles are much larger than the size of the Sn@C nanoparticles. (ii) While the dimensions of the carbon coated nanowires are of the same order as the Sn@C nanoparticles, the nanowires were discharged over just 20 s, as opposed to the tens of hours used for the Sn@C-GNs. Given that both Li and Sn are fast diffusers, it appears likely that the extremely slow discharge rate used here for Sn@C-GNs leads to nearly equilibrium products, though it is possible for some redistribution in the time period between electrochemistry and ex situ observation. The high-resolution ⁷Li NMR data provides an interesting complement to diffraction studies, while also providing new information that is unavailable from those techniques.

¹³C NMR of Graphene Nanosheets. Before discussing the ¹³C NMR investigation of the hybrid anode, we investigate the graphene nanosheets interconnecting the nanoparticles in Sn@C-GNs and discuss the benefits demonstrated by the CPMG-MAS experiments benchmarked on this system. A schematic structure of graphene,[6−8] formed via reduction of graphene oxide, is shown in Figure 4a. The ¹³C CPMG-MAS spectrum of
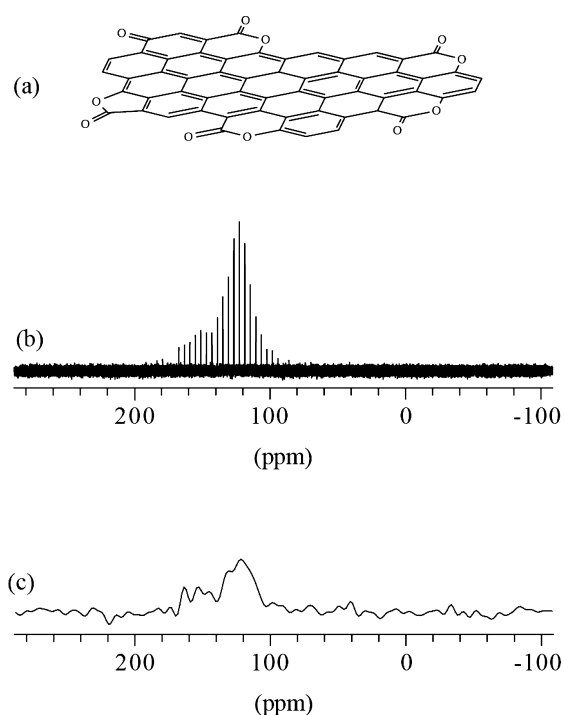

Figure 4. (a) Schematic of the studied GNs, showing incomplete reduction of the edge groups.[8] (b) ¹³C CPMG-MAS NMR spectrum of GNs. (c) Bloch decay version of the spectrum in (b).

powdered graphene nanosheets (GNs) is displayed in Figure 4b, and it should be noted that each spikelet is not an individual site; rather, it is the tops of the spikelets that encode the line shape. The predominantly sp² character of the GNs is clear in the 120 ppm center of gravity of the peak. The line shape is ∼70 ppm wide at its base, reflecting a wide variation in chemical shifts and, therefore, chemical environments. Interestingly, this width is related to a large variety of edge terminations, as the high-frequency weighting of the line shape indicates that some of the graphene oxide edge groups[8] are not fully reduced. Comparison to spectra of the graphene oxide starting material[6,8] is consistent with the simplified chemical speciation upon reduction and mirrors published data collected using conventional Bloch-decay experiments acquired on large sample volumes.[8,26−33] Conversely, the CPMG-MAS

results shown in Figure 4b were obtained using just a few mg of material. The equivalent Bloch decay version of the spectrum is shown in Figure 4c and is of such reduced signal intensity that it is difficult to confidently separate it from artifact signals.

It is worth discussing some of the details of the ¹³C CPMG-MAS method, given the information content typical for ¹³C spectra[6−11] and the fact that the experiments presented below were found to be unworkable without the CPMG-MAS method. The difficulty of studying technological carbonaceous materials is exacerbated in materials such as Sn@C-GNs, where the relevant sites are without protons (prohibiting ¹H−¹³C cross-polarization signal enhancement), and disorder or heterogeneity is likely to spread the available signal intensity over multiple broad peaks. We point out here that this is the ideal situation for maximum enhancement by continual signal refocusing and observation in an echo train, i.e., using the CPMG method.[4,5] CPMG applied under magic-angle spinning (MAS) is useful when there is a distribution of frequencies that are not refocused by MAS, but which can be refocused by rf pulses.[34−38] CPMG has been applied in a few cases to enhance the ¹³C NMR spectra from static (or static-like, slow-spinning) samples,[39−43] and has also been employed to compress a range of ¹³C chemical shifts into a single spikelet to speed its recording.[44] However, the use of CPMG to enhance ¹³C spectra by refocusing large distributions of isotropic ¹³C chemical shifts, which cannot be refocused by MAS, appears to have gone undeveloped. Likely, this is because the large MAS line widths of complex samples and the long spin-state lifetimes of graphitic carbons are underappreciated, while this ratio of properties is exactly where large CPMG enhancements are possible. See the Supporting Information for a more detailed discussion of the CPMG pulse sequence and methodology.

¹³C NMR of Sn@C-GNs. The ¹³C CPMG-MAS line shape of the composite material, Figure 5a, is much broader than that of the pristine GNs; however, its similar 120 ppm average chemical shift also reflects primarily sp² hybridized carbons. It should be noted that the graphene sheets are only a few atomic layers thick, so nearly the entire peak intensity is derived from the 50 nm thick carbon shells. There is no evidence of distinct secondary sites in the line shape, so its breadth likely results from disorder in bond lengths and angles of the sp² sites and may also reflect smaller contributions from oxygen functionalities similar to those seen in graphene oxide[6,8] or sp³ hybridized carbons.[9−11] It is also quite likely that bulk magnetic susceptibility broadening[45−47] plays some role in the line widths observed here.

The CPMG-MAS time-domain signal for the Sn@C-GNs composite, Figure 6a, shows that the signal is observed as a series of 1900 echoes over a remarkably long period of 3.75 s, with a relaxation time constant, T_2, value of 0.79(1) seconds. In a rigid solid such as the sp² carbon layer of Sn@C-GNs, long nuclear-spin-state lifetimes might be expected; however, the
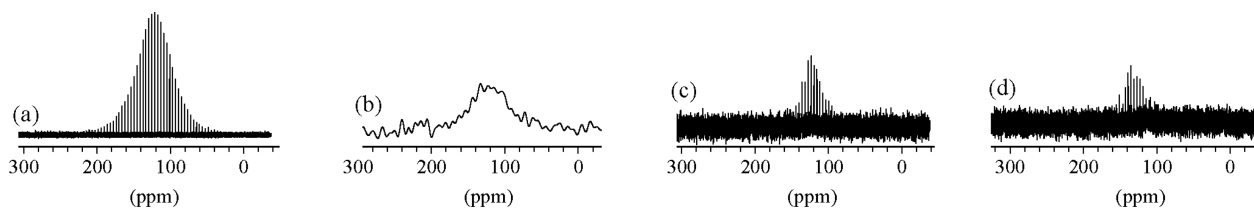

Figure 5. (a, b) Carbon-13 CPMG-MAS NMR and Bloch decay spectra of pristine Sn@C-GNs. (c, d) Carbon-13 CPMG-MAS NMR spectrum of ex situ powdered Sn@C-GNs electrodes after electrochemical discharge to 0.4 V vs Li/Li⁺ in (c) and 0.01 V in (d).
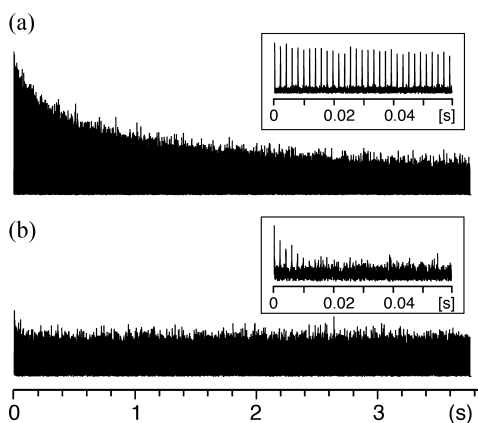
Figure 6. Time-domain data from ^{13}C CPMG-MAS NMR experiments carried out on the Sn@C-GNs composite, with insets showing expansions of the first 60 ms. (See Figure 5a,c for the corresponding spectra.)

signal observation at evolution times beyond 3.5 s is incredible. The ^{13}C MAS spectrum, i.e., that obtained by Fourier transformation of the first echo of the CPMG-MAS echo train, is shown in Figure 5b. The conventional MAS spectrum is barely above the threshold for detection with a S/N of 5, while the CPMG version exhibits a significant enhancement to a S/N of 90, representing an efficiency boost on the order of months.

^{13}C CPMG-MAS NMR spectra of the charged Sn@C-GNs samples are shown in Figure 5c,d. The time-domain data from the NMR experiment in Figure 5c is shown in Figure 6b. The ability to record these challenging spectra demonstrates the increased reach of ^{13}C CPMG-MAS over Bloch-decay experiments. The average chemical shift is relatively unchanged from the pristine material; however, there is a significant change in the lifetime of the ^{13}C transverse magnetization, which is reduced by more than 2 orders of magnitude ($T_2 = 5.6(8)$ and $1.0(2)$ milliseconds for the 0.4 and 0.01 V samples, respectively). The loss of S/N reflects an extreme change in the ability to refocus the ^{13}C signal over hundreds of echoes, due to the substantial reduction in T_2. Obviously, the rapid relaxation is induced by the electrochemically added electrons. It is particularly interesting that both sample's carbon T_2 values are affected, as the sample that was halted at 0.4 V is shown by ^7Li NMR to be reduced chiefly at the metallic tin core, with no ^7Li observation of interaction between the carbon itself and the inserted lithium ions. In contrast, the electrons that are inserted into the material are observed homogeneously across the carbon shell, via the uniform ^{13}C relaxation effects. It is possible that the reduced core of the nanoparticles interacts cooperatively with the carbon shell, sharing electrons with this neighboring component.

^{13}C NMR of Li−O$_2$ Cell Electrodes. Given the novelty of the ^{13}C CPMG-MAS measurements on Sn@C-GNs, a second material was investigated to provide more insight into the meaning of the data collected. The graphitic carbon electrodes used in Li−O$_2$ batteries, which theoretically possess a greater energy density than gasoline, were used as a contrasting system.[12,13] In these cells, the role of the carbon is as a porous, conductive host, to support the Li$^+$ and peroxide radical chemistry, which ideally produces Li$_2$O$_2$ on the surface of the carbon.[12,13] Unfortunately, poor understanding and control of the electrochemical reactions of electrons at the graphite surface with the intended reductant (solubilized O$_2$) and with

undesirable components (electrolytes in particular) is one of the impediments to commercialization.[12] Because of the critical role of graphite in this process, we have applied ^{13}C CPMG-MAS NMR spectroscopy to the graphite layer of functioning Li−O$_2$ cells to search for changes during the electrochemical cycle.

The ^{13}C CPMG-MAS spectrum of a pristine carbon-black electrode is shown in Figure 7b. The 120 ppm average chemical
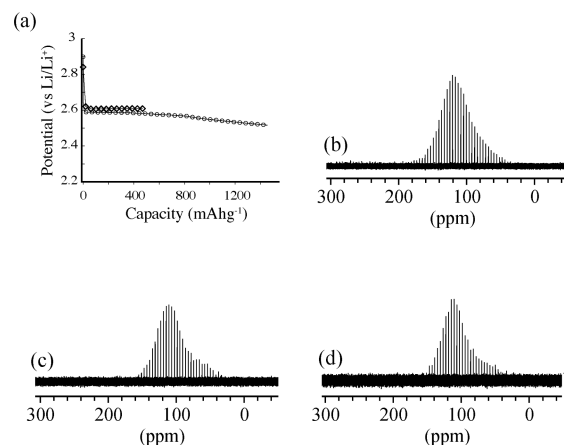

Figure 7. (a) Discharge voltage profiles for the two Li−O$_2$ cells studied here. (b−d) Carbon-13 CPMG-MAS NMR spectra of carbon black electrodes: (b) an assembled, but unused, cell; (c) discharged to a capacity of 490 mAhg^{-1}; (d) discharged to 1450 mAhg^{-1}.

shift of the broad peak is in line with the average shifts of the GNs and the Sn@C-GNs composite. The width of the peak is also similar to that of Sn@C-GNs, though the distribution has more intensity on the low frequency side, possibly reflecting more sites in the carbon-black sample being less graphitic and possessing greater sp^3 character. As observed in the experiments on the GNs and Sn@C-GNs, the ^{13}C coherence lifetime of the carbon in this cathode is very long, $T_2 = 0.43(2)$ seconds, and provides a large signal enhancement.

The ^{13}C CPMG-MAS spectra of samples of this type of carbon black electrode charged to a capacity of 490 and 1450 mAhg^{-1} (Figure 7a) in a Li−O$_2$ cell in a pure O$_2$ environment (0.26 and 1.32 mg of Li$_2$O$_2$ per mg of carbon black) are shown in Figure 7c,d, respectively. The charging process again induces no significant change in the carbon chemical shifts or overall line shape. However, in stark contrast to the Sn@C-GNs electrode, the transverse relaxation time is unchanged by the electrochemical reaction ($T_2 = 0.39(3)$ and $0.32(6)$ s for the 490 and 1450 mAhg^{-1} samples, respectively). The critical difference between the two types of electrodes is that the carbon black is acting as a spectator in the Li−O$_2$ cell, serving only as a charge carrier during the reaction, while in the Sn@C-GNs cell, the carbon is directly involved in the reaction.

■ CONCLUSIONS

This report demonstrates new and detailed information on electrochemical processes in electrodes, including information from experimental methods developed herein. ^7Li NMR is used to study the state of charge of a lithium-battery anode, and 2D ^7Li EXSY experiments provide a model of the multistep reduction process by measuring the proximity of the various reduced species. We show that ^{13}C CPMG-MAS NMR encodes the chemical environment while providing a remarkable signal

enhancement. In addition to the sensitivity of the ^{13}C chemical shifts, the inherently included relaxation data provides a further characterization vector. Given the ease of implementing ^{13}C CPMG experiments, we anticipate future applications include many important carbonaceous materials. The localized nature of the measurements used provide important insight into the species formed during the electrochemical reactions in the various components of the heterogeneous electrode materials.

■ ASSOCIATED CONTENT

Ⓢ Supporting Information

Further details on the T$_2$-filtering of ^{7}Li signals from the SEI and an example spectrum. Details on the CPMG-MAS method, its implementation, and key references. This material is available free of charge via the Internet at http://pubs.acs.org.

■ AUTHOR INFORMATION

Corresponding Author
*E-mail: goward@mcmaster.ca.

Notes
The authors declare no competing financial interest.

■ ACKNOWLEDGMENTS

■ REFERENCES

(1) Beaulieu, L. Y.; Eberman, K. W.; Turner, R. L.; Krause, L. J.; Dahn, J. R. *Electrochem. Solid-State Lett.* **2001**, *4*, A137.

(2) Timmons, A.; Dahn, J. R. *J. Electrochem. Soc.* **2006**, *153*, A1206.

(3) Wang, D.; Li, X.; Yang, J.; Wang, J.; Geng, D.; Li, R.; Cai, M.; Sham, T.-K.; Sun, X. *Phys. Chem. Chem. Phys.* **2013**, *15*, 3535.

(4) Carr, H. Y.; Purcell, E. M. *Phys. Rev.* **1954**, *94*, 630.

(5) Meiboom, S.; Gill, D. *Rev. Sci. Instrum.* **1958**, *29*, 688.

(6) Cai, W.; Piner, R. D.; Stadermann, F. J.; Park, S.; Shaibat, M. A.; Ishii, Y.; Yang, D.; Velamakanni, A.; An, S. J.; Stoller, M.; An, J.; Chen, D.; Ruoff, R. S. *Science* **2008**, *321*, 1815.

(7) Lerf, A.; He, H. Y.; Forster, M.; Klinowski, J. *J. Phys. Chem. B* **1998**, *102*, 4477.

(8) Gao, W.; Alemany, L. B.; Ci, L.; Ajayan, P. M. *Nat. Chem.* **2009**, *1*, 403.

(9) Fang, X.; Mao, J.; Levin, E. M.; Schmidt-Rohr, K. *J. Am. Chem. Soc.* **2009**, *131*, 1426.

(10) Alam, T. M.; Friedmann, T. A.; Schultz, P. A.; Sebastiani, D. *Phys. Rev. B* **2003**, *67*, 245309.

(11) Golzan, M. M.; Lukins, P. B.; McKenzie, D. R.; Vassallo, A. M.; Hanna, J. V. *Chem. Phys.* **1995**, *193*, 167.

(12) Bruce, P. G.; Freunberger, S. A.; Hardwick, L. J.; Tarascon, J.-M. *Nat. Mater.* **2012**, *11*, 19.

(13) Kraytsberg, A.; Ein-Eli, Y. *J. Power Sources* **2011**, *196*, 886.

(14) Bekaert, E.; Robert, F.; Lippens, P. E.; Menetrier, M. *J. Phys. Chem. C* **2010**, *114*, 6749.

(15) Furuya, K.; Ogawa, K.; Mineo, Y.; Matsufuji, A.; Okuda, J.; Erata, T. *J. Phys.: Condens. Matter* **2001**, *13*, 3519.

(16) Zaghib, K.; Tatsumi, K.; Sawada, Y.; Higuchi, S.; Abe, H.; Ohsaki, T. *J. Electrochem. Soc.* **1999**, *146*, 2784.

(17) Hayes, S. E.; Guidotti, R. A.; Even, W. R.; Hughes, P. J.; Eckert, H. *J. Phys. Chem. A* **2003**, *107*, 3866.

(18) Wang, Y.; Yufit, V.; Guo, X.; Peled, E.; Greenbaum, S. *J. Power Sources* **2001**, *94*, 230.

(19) Letellier, M.; Chevallier, F.; Clinard, C.; Frackowiak, E.; Rouzaud, J.-N.; Béguin, F. *J. Chem. Phys.* **2003**, *118*, 6038.

(20) Meyer, B. M.; Leifer, N.; Sakamoto, S.; Greenbaum, S. G.; Grey, C. P. *Electrochem. Solid-State Lett.* **2005**, *8*, A145.

(21) Beaulieu, L. Y.; Beattie, S. D.; Hatchard, T. D.; Dahn, J. R. *J. Electrochem. Soc.* **2003**, *150*, A419.

(22) Chao, S. C.; Song, Y. F.; Wang, C. C.; Sheu, H. S.; Wu, H. C.; Wu, N. L. *J. Phys. Chem. C* **2011**, *115*, 22040.

(23) Chao, S. C.; Yen, Y. C.; Song, Y. F.; Chen, Y. M.; Wu, H. C.; Wu, N. L. *Electrochem. Commun.* **2010**, *12*, 234.

(24) Li, Q. Q.; Wang, P.; Feng, Q.; Mao, M. M.; Liu, J. B.; Mao, S. X.; Wang, H. T. *Chem. Mater.* **2014**, *26*, 4102.

(25) Rhodes, K. J.; Meisner, R.; Kirkham, M.; Dudney, N.; Daniel, C. *J. Electrochem. Soc.* **2012**, *159*, A294.

(26) Lambert, T. N.; Luhrs, C. C.; Chavez, C. A.; Wakeland, S.; Brumbach, M. T.; Alam, T. M. *Carbon* **2010**, *48*, 4081.

(27) Liu, H.; Zhang, L.; Guo, Y.; Cheng, C.; Yang, L.; Jiang, L.; Yu, G.; Hu, W.; Liu, Y.; Zhu, D. *J. Mater. Chem. C* **2013**, *1*, 3104.

(28) Panich, A. M.; Shames, A. I.; Aleksenskii, A. E.; Dideikin, A. *Solid State Commun.* **2012**, *152*, 466.

(29) Park, S.; Hu, Y.; Hwang, J. O.; Lee, E.-S.; Casabianca, L. B.; Cai, W.; Potts, J. R.; Ha, H.-W.; Chen, S.; Oh, J.; Kim, S. O.; Kim, Y.-H.; Ishii, Y.; Ruoff, R. S. *Nat. Commun.* **2012**, *3*, 638.

(30) Si, Y.; Samulski, E. T. *Nano Lett.* **2008**, *8*, 1679.

(31) Stankovich, S.; Dikin, D. A.; Piner, R. D.; Kohlhaas, K. A.; Kleinhammes, A.; Jia, Y.; Wu, Y.; Nguyen, S. T.; Ruoff, R. S. *Carbon* **2007**, *45*, 1558.

(32) Vernekar, A. A.; Mugesh, G. *Chem.—Eur. J.* **2013**, *19*, 16699.

(33) Wang, X.; Hu, Y.; Song, L.; Yang, H.; Xing, W.; Lu, H. *J. Mater. Chem.* **2011**, *21*, 4222.

(34) Vosegaard, T.; Larsen, F. H.; Jakobsen, H. J.; Ellis, P. D.; Nielsen, N. C. *J. Am. Chem. Soc.* **1997**, *119*, 9055.

(35) Larsen, F. H.; Farnan, I. *Chem. Phys. Lett.* **2002**, *357*, 403.

(36) Hou, S. S.; Beyer, F. L.; Schmidt-Rohr, K. *Solid State Nucl. Magn. Reson.* **2002**, *22*, 110.

(37) Trebosc, J.; Wiench, J. W.; Huh, S.; Lin, V. S. Y.; Pruski, M. *J. Am. Chem. Soc.* **2005**, *127*, 7587.

(38) Wiench, J. W.; Lin, V. S. Y.; Pruski, M. *J. Magn. Reson.* **2008**, *193*, 233.

(39) Szeverenyi, N. M.; Bax, A.; Maciel, G. E. *J. Magn. Reson.* **1985**, *61*, 440.

(40) Shore, S. E.; Ansermet, J. P.; Slichter, C. P.; Sinfelt, J. H. *Phys. Rev. Lett.* **1987**, *58*, 953.

(41) Desoto, S. M.; Slichter, C. P.; Kini, A. M.; Wang, H. H.; Geiser, U.; Williams, J. M. *Phys. Rev. B* **1995**, *52*, 10364.

(42) Hu, J. Z.; Wind, R. A. *J. Magn. Reson.* **2003**, *163*, 149.

(43) Gowda, C. M.; Agarwal, V.; Kentgens, A. P. M. *J. Magn. Reson.* **2012**, *223*, 11.

(44) Farooq, H.; Courtier-Murias, D.; Soong, R.; Masoom, H.; Maas, W.; Fey, M.; Kumar, R.; Monette, M.; Stronks, H.; Simpson, M. J.; Simpson, A. J. *Magn. Reson. Chem.* **2013**, *51*, 129.

(45) Alla, M.; Lippmaa, E. *Chem. Phys. Lett.* **1982**, *87*, 30.

(46) Schwerk, U.; Michel, D.; Pruski, M. *J. Magn. Reson., Ser. A* **1996**, *119*, 157.

(47) Vanderhart, D. L.; Earl, W. L.; Garroway, A. N. *J. Magn. Reson.* **1981**, *44*, 361.